Variable Temporal Resolution Reconstruction for Golden-Angle Radial Sparse Parallel DCE-MRI

Robert Grimm[1], Dominik Nickel[2], Jana Hutter[1], Christoph Forman[1], Berthold Kiefer[2], Joachim Hornegger[1], and Kai Tobias Block[3]
[1]*Pattern Recognition Lab, FAU Erlangen-Nuremberg, Erlangen, Germany,* [2]*MR Application Development, Siemens AG, Healthcare Sector, Erlangen, Germany,*
[3]*Department of Radiology, NYU Langone Medical Center, New York City, New York, United States*

INTRODUCTION: Novel methods for dynamic contrast-enhanced MR imaging (DCE-MRI) such as the Golden-angle RAdial Sparse Parallel (GRASP) technique [1] achieve a high temporal resolution by exploiting correlations between different imaging time points. Typically, the reconstructed time points are distributed with equal distance, which is not always the optimal strategy. For example, in perfusion measurements, high temporal resolution is most relevant in the initial phase after the contrast injection, but less important before the injection and in later phases. In order to reduce the vast number of images that need to be processed, stored, and evaluated, this work describes a modified reconstruction approach in which image time points may have variable temporal resolution and non-uniform distance. In this way, the total number of images can be reduced significantly while application-relevant timing requirements are maintained, which results in considerably shorter reconstruction time.

THEORY: For radial k-space acquisitions with the golden-angle ordering scheme [2] as employed by GRASP, temporal frames can be formed by grouping an arbitrary number of consecutively acquired radial spokes. Hence, the temporal resolution of a reconstructed image frame can be chosen freely and is essentially only limited by the tolerable degree of undersampling [3,4]. In GRASP, all image frames are calculated simultaneously using an iterative reconstruction that applies a total-variation (TV) constraint along the temporal dimension to remove the "flickering" undersampling artifacts that appear for high temporal resolutions, based on the a priori knowledge that true intensity changes caused by the contrast agent do not lead to distinct image flickering. The series of image frames is reconstructed by minimizing the cost function:

$$\hat{\boldsymbol{x}} = \arg_{\boldsymbol{x}} \min \left(\sum_{t=1}^{T} \omega_t \|\boldsymbol{A}_t \boldsymbol{x}_t - \boldsymbol{y}_t\|_2^2 + \sum_{t=1}^{T-1} \lambda_t \|\boldsymbol{x}_{t+1} - \boldsymbol{x}_t\|\right).$$

Here, $\boldsymbol{x}$ denotes the 2D+t image volume to be estimated, $\boldsymbol{x}_t$ the respective image frame at time t, and $\boldsymbol{y}_t$ the k-space raw data grouped for time frame t, which includes data from different coils. The k-space encoding operator (or "forward" operator) is denoted as $\boldsymbol{A}_t$ and includes multiplication with coil-sensitivity profiles, FFT, and sampling along the radial spokes that were grouped for time t. When using equidistant time points with equal window size, a fixed value can be used for the scaling factor λ_t, and ω_t can be set to 1. However, when varying the window width for different time points, it is necessary to adapt the scaling factors ω_t and λ_t in order to account for the variable amount of k-space data grouped for the different time points. Thus, the scaling factor ω_t should be selected inversely proportional to the number of spokes grouped for time frame t to normalize the impact that each image frame has on the cost function. Both scaling factors could also be combined into a single coefficient, but separate coefficients for the k-space data fidelity and regularization make it easier to maintain a similar level of temporal regularization among reconstructions with different time-point configuration.

EXPERIMENTS: Retrospective reconstructions of IRB-approved patient measurements were performed, which were previously acquired with a 1.5T system (Siemens MAGNETOM Avanto) for the liver (D1) and with a 3T system (Siemens MAGNETOM Trio) for the prostate (D2) using a radial stack-of-stars 3D GRE sequence. Protocol parameters included 2104 radial spokes, 256 pixel base resolution, 64 slices, 337 sec scan time, 39x39x19 cm^3 FOV for D1 and 3128 radial spokes, 228 pixel base resolution, 24 slices, 338 sec scan time, 24x24x7 cm^3 FOV for D2. Three reconstructions were computed for each dataset: R_{21} with fixed temporal resolution of 21 spokes / frame, R_{84} with 84 spokes / frame, and $R_{21/84}$ using the proposed approach with 21 spokes / frame for the first 40 frames and 84 spokes / frame for the remaining frames. This corresponds to temporal resolutions of 3.4 s / 13.5 s (D1) and 2.2 s / 8.9 s (D2). For the variable reconstruction $R_{21/84}$, a weight of ω_t=1/4 was applied for all time frames composed of 84=4*21 spokes to compensate for the 4-times larger data amount per frame. For the fixed reconstructions R_{21} and R_{84}, ω_t =1 was used for all time frames. The regularization coefficient was set to $\lambda_t = \omega_t * \lambda$, where λ=2.0 was the weight used in the conventional reconstructions. For all three reconstructions, the computation time was estimated. Furthermore, the accuracy of the variable reconstruction was analyzed by computing the relative difference in both segments t =1...40 and t =41…T, where the corresponding frames of R_{21} and R_{84} served as the reference, respectively. To eliminate bias by low-intensity areas, only pixel locations were considered where the signal intensity was higher than the mean intensity in R_{21} and R_{84}.

RESULTS AND DISCUSSION: As listed in Table 1, the total reconstruction time using a prototypical GRASP implementation in C++ was reduced from 161 min to 100 min for the liver dataset from and 59 min to 32 min for the prostate dataset. While the reconstruction effort from the radial gridding operations remains unchanged, this acceleration results from the reduced number of time points that linearly contribute to the number of FFTs in the encoding operator $\boldsymbol{A}$ as well as to the computation of the finite differences for the regularization. Instead of 100 (D1) and 152 frames (D2) in R_{21}, only 55 and 68 frames were generated in the variable reconstruction. Fig. 1 shows that the resulting temporal resolution in the initial uptake phase is almost identical in R_{21} and $R_{21/84}$, while in the second segment R_{84} and $R_{21/84}$ match very closely. This was also confirmed in the quantitative evaluation with a mean deviation of less than 3.4 % in the first segment and less than 1.2 % in the second segment.

Dataset	Reconstruction Time			Mean Difference	
	R_{21}	R_{84}	$R_{21/84}$	Segment 1	Segment 2
D1 (Liver)	161 min	67 min	100 min	1.6 ± 1.8 %	0.8 ± 0.1 %
D2 (Prostate)	59 min	25 min	32 min	3.4 ± 3.0 %	1.2 ± 1.1 %

Table 1: Reconstruction times for fixed temporal resolution reconstructions R_{21}, R_{84} and the proposed method $R_{21/84}$, as well as mean difference in the two segments.

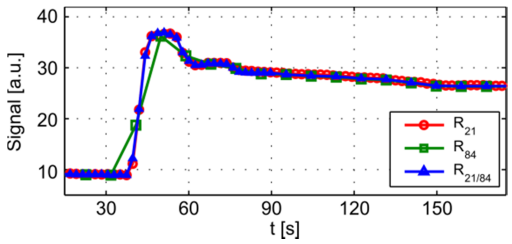

Fig. 1: Time intensity curve in a ROI in the aorta (D2).

CONCLUSION: Reconstruction of time frames with variable temporal resolution can be used to reduce the computational burden of iterative DCE-MRI techniques such as GRASP without sacrificing clinical timing requirements. By using a high temporal resolution in only the first ~90 s of a perfusion measurement and using a lower temporal resolution afterwards, it was possible to reduce the reconstruction time by 38 – 46 % in the cases tested in this work without evident loss of relevant temporal information. The number of reconstructed images was reduced by 45 – 55 %, which additionally lowers the IT resources needed for evaluating and storing such studies in clinical practice. In the current work, segments with variable temporal resolution were defined manually. Based on an automatic bolus-detection mechanism that we have previously described for the same type of acquisition [5], it may be possible to determine optimal segment boundaries adaptively without any user interaction.

REFERENCES: [**1**] Feng et al, MRM, doi: 10.1002/mrm.24980, in press, 2013. [**2**] Winkelmann IEEE TMI 26, p68, 2007.
[**3**] Lin et al, MRM 60, p1135, 2008. [**4**] Chan et al, MRM 67, 2012. [**5**] Grimm et al, #0696, Proc. ISMRM 2013.